Cell, Vol. 108, 57–70, January 11, 2002, Copyright ©2002 by Cell Press

Mechanism of c-Myb–C/EBPβ Cooperation from Separated Sites on a Promoter

Tahir H. Tahirov,[1,2,9,11] Ko Sato,[1,3] Emi Ichikawa-Iwata,[6] Motoko Sasaki,[1,2,9] Taiko Inoue-Bungo,[1,2] Masaaki Shiina,[1,4] Kazumi Kimura,[1,2] Shioka Takata,[3] Atsushi Fujikawa,[1,5] Hisayuki Morii,[8] Takashi Kumasaka,[10] Masaki Yamamoto,[10] Shunsuke Ishii,[6,7] and Kazuhiro Ogata[1,2,3,9,11]

[1] Kanagawa Academy of Science and Technology (KAST)
3-9 Fukuura
Kanazawa-ku
Yokohama 236-0004
Japan
[2] Department of Structural Biology
[3] Department of Biochemistry
[4] Department of Pathology
[5] Department of Urology
Yokohama City University School of Medicine
3-9 Fukuura
Kanazawa-ku
Yokohama 236-0004
Japan
[6] Laboratory of Molecular Genetics
RIKEN Tsukuba Institute
[7] CREST (Core Research for Evolutional Science and Technology) Research Project of JST (Japan Science and Technology Corporation)
3-1-1 Koyadai
Tsukuba
Ibaraki 305-0074
Japan
[8] Protein Dynamics Group
National Institute of Advanced Industrial Science and Technology
Central 6
1-1-1 Higashi
Tsukuba
Ibaraki 305-8566
Japan
[9] Bio-Crystallography Technology Division
[10] Structural Biophysics Laboratory
RIKEN Harima Institute / SPring-8
1-1-1 Kouto
Mikazuki
Sayo
Hyogo 679-5148
Japan

Summary

c-Myb, but not avian myeloblastosis virus (AMV) v-Myb, cooperates with C/EBPβ to regulate transcription of myeloid-specific genes. To assess the structural basis for that difference, we determined the crystal structures of complexes comprised of the c-Myb or AMV v-Myb DNA-binding domain (DBD), the C/EBPβ DBD, and a promoter DNA fragment. Within the c-Myb complex, a DNA-bound C/EBPβ interacts with R2 of c-Myb bound to a different DNA fragment; point mutations in v-Myb R2 eliminate such interaction within the v-Myb complex. GST pull-down assays, luciferase *trans*-activation assays, and atomic force microscopy confirmed that the interaction of c-Myb and C/EBPβ observed in crystal mimics their long range interaction on the promoter, which is accompanied by intervening DNA looping.

[11] Correspondence: ogata@med.yokohama-cu.ac.jp [K.O.]; tahir@med.yokohama-cu.ac.jp [T.H.T.]

Introduction

Assembly of stereospecific, multiprotein complexes on enhancers and promoters is a key step in transcriptional activation (Tjian and Maniatis, 1994). Recent X-ray analyses of high-order complexes comprised of transcription factors bound to DNA have concentrated exclusively on cases in which interactions between transcription factors enable or enhance their cooperative binding to adjacent sites on a promoter (Wolberger, 1998). In many eukaryotic genes, however, transcription factors bind to promoters at sites distant from one another, yet act synergistically to activate transcription (Carey, 1998). It has been proposed that DNA looping mediated by their interaction brings transcription factors scattered along the DNA into sufficiently close proximity to enable them to form nucleoprotein complexes (Schleif, 1992). Thus far, however, there is very little structural evidence on an atomic scale that explains the synergistic *trans*-activation by distantly separated transcription factors. For example, it was modeled that an oligomerization domain separated from a DNA-binding domain acts as an inducer of DNA looping in the case of *lac* repressor-promoter DNA interaction (Friedman et al., 1995). Here, we address this problem in the case of the synergistic *trans*-activation of myeloid genes by c-Myb and C/EBPβ.

The c-*myb* proto-oncogene product (c-Myb) is an essential regulator of proliferation and differentiation of hematopoietic cells (Lipsick and Wang, 1999). c-Myb acts as a transcriptional regulatory factor (Weston and Bishop, 1989; Ness et al., 1989; Sakura et al., 1989), modulating expression of various target genes in the hematopoietic system, in many cases with cooperation of a wide variety of other transcriptional regulatory factors, including members of the CAAT-enhancer binding protein (C/EBP) family, the Ets family, and core binding factors (CBFs) (Ness, 1999). In particular, C/EBP family members (C/EBPα, C/EBPβ, C/EBPδ, and C/EBPϵ) are frequently observed and well-characterized c-Myb partners, regulating transcription of such hematopoietic genes as *mim-1* (Ness et al., 1993; Burk et al., 1993), lysozyme (Ness et al., 1993), *tom-1A* (Burk et al., 1997), myeloperoxidase (MPO) (Bristos-Bray and Friedman, 1997), neutrophil elastase (Oelgeschläger et al., 1996;

Verbeek et al., 1999), RAG2 (Fong et al., 2000), and myeloblastin (Lutz et al., 2001). Indeed, ectopic expression of Myb and C/EBPs in heterologous cell types induces endogenous markers of myeloid differentiation, including *mim-1* and lysozyme genes (Ness et al., 1993).

Two oncogenic viral forms of Myb encoded by the AMV and E26 viruses (AMV v-Myb and E26 v-Myb) are also known (Lipsick and Wang, 1999). The N- and C-terminal regions of both v-Myb proteins are truncated relative to c-Myb. Like c-Myb, E26 v-Myb activates granulocyte-specific genes, including *mim-1*, whereas AMV v-Myb does not (Ness et al., 1989; Introna et al., 1990; Kowenz-Leutz et al., 1997). Moreover, the phenotypes of myeloid cells transformed by E26 and AMV differ: the former resemble myeloblasts, while the latter resemble monoblasts (Introna et al., 1990). These differences were attributed to multiple point mutations found in the DBD of AMV v-Myb, which affect the transcription of unique sets of differentiation-specific genes.

The DBD of c-Myb consists of three imperfect tandem repeats of 51 or 52 amino acid residues, referred to as R1, R2, and R3 from the N terminus (Kanei-Ishii et al., 1990). Our previous analyses of the structures in solution using nuclear magnetic resonance (NMR) spectroscopy revealed that each repeat contains three helices (α1, α2, and α3) with the helix-turn-helix variant motif (Ogata et al., 1992, 1995), and that R2 and R3 are involved in specific DNA recognition, while R1 loosely covers the DNA position next to the R2 binding site (Ogata et al., 1994, 1995). The structure of R2 also contains a partially exposed hydrophobic patch (Ogata et al., 1995); within the corresponding region of the AMV v-Myb DBD, this hydrophobic patch contains the three point mutations responsible for the failure of v-Myb to activate the *mim-1* promoter (Ness et al., 1989; Introna et al., 1990; Ogata et al., 1995; Kowenz-Leutz et al., 1997), suggesting that this hydrophobic patch is important for the interaction of c-Myb and C/EBPβ and for their synergistic activation of transcription.

To establish the structural basis for the synergy between c-Myb and C/EBPβ and its disruption by the mutations found in the AMV v-Myb DBD, we determined the crystal structures of ternary complexes containing the c-Myb or AMV v-Myb DBD, the C-terminal portion of C/EBPβ, including the DBD, and a DNA fragment from the *tom-1*A promoter: c-Myb$_{38\text{-}193}$–C/EBP$\beta_{259\text{-}336}$–DNA, c-Myb$_{38\text{-}193}$–C/EBP$\beta_{273\text{-}336}$–DNA, and AMV v-Myb$_{66\text{-}193}$–C/EBP$\beta_{259\text{-}336}$–DNA are respectively named c-Myb complex I, c-Myb complex II (or generally c-Myb complex without discrimination of complexes I and II), and v-Myb complex. We found that the c-Myb complex shows specific intercomplex binding between c-Myb and C/EBPβ, which is not shown by the v-Myb complex, and which was confirmed in solution using GST pull-down assays. This interaction between c-Myb and C/EBPβ allowed us to speculate that, via DNA looping, c-Myb and C/EBPβ are able to interact and cooperate despite the fact that they bind to natural promoters at some distance from one another. We then used atomic force microscopy (AFM) to confirm that c-Myb and C/EBPβ could interact through looping of the *mim-1* promoter and showed its functional relevance, in vivo, using a luciferase *trans*-activation assay.

Results and Discussion

Overview of the Crystal Structures of the c-Myb and v-Myb Complexes

Figures 1A–1C show the crystal structure of c-Myb complex I. In both c-Myb and v-Myb complexes, the contiguous DNA fragments form a pseudocontinuous double-stranded DNA related by a 2-fold screw axis. Within the c-Myb complex, the DNA fragments are bent significantly (Figure 1A), while DNA bending in the v-Myb complex is slight. The R1, R2, and R3 of c-Myb form three tandemly linked globular subdomains and bind to the DNA mainly in the major groove (Figures 1A–1C). Within c-Myb complex I, R1 also approaches the N-terminal portion of a C/EBPβ bZip region from an adjoining complex, forming one hydrogen bond and two van der Waals contacts. This intermolecular interaction appears weak, however, and is probably not functionally important, since it is lost in c-Myb complex II, causing the R1 domain to become unfixed. Within the v-Myb complex, R2 and R3 form two tandemly linked globular subdomains that bind to the DNA as in the c-Myb complex; R1 is truncated, however, and what remains is structurally disordered.

Like other bZip type protein–DNA complexes, C/EBPβ C-terminal fragments containing the bZip region form homodimers with a coiled-coil structure at the leucine zipper parts and bind to the DNA major groove at the basic regions of the fragments in both c-Myb and v-Myb complexes. C/EBPβ–DNA interactions are similar within c-Myb and v-Myb complexes and are not discussed here due to space limitations. It is noteworthy, however, that only within the c-Myb complex does the C-terminal leucine zipper region of a C/EBPβ molecule bound to one DNA fragment interact with a c-Myb molecule bound to another DNA fragment. Moreover, this interaction persists in crystal systems containing C/EBPβ molecules of differing lengths—i.e., c-Myb complexes I and II. On the other hand, there is no interaction between C/EBPβ and AMV v-Myb within the v-Myb complex.

Specific DNA Recognition by c-Myb and AMV v-Myb

c-Myb and v-Myb specifically bind to the consensus sequence 5′-YAACNG-3′ (Y and N indicate a pyrimidine and any base, respectively) (Biedenkapp et al., 1988; Tanikawa et al., 1993; Ogata et al., 1996; Oda et al., 1997), though the interaction is also affected by the consensus site's 3′ flanking sequence (Nakagoshi et al., 1990; Howe and Watson, 1991; Weston, 1992; Ording et al., 1994; Ganter et al., 1999). The mode of DNA recognition by c-Myb R2R3 was determined previously using a heteronuclear multidimensional NMR (Ogata et al., 1994); the crystal structures presented here revealed novel features about the protein-DNA interface, which were not identified in the NMR structure due to the line broadening effect of the signals from the protons at the interface or water-mediated interactions.

The c-Myb–DNA and v-Myb–DNA interactions shown schematically in Figures 2A and 2B, respectively, reveal that c-Myb and v-Myb recognize DNA in similar fashion. The structural details of the specific c-Myb–DNA interactions are presented in Figure 2C. Asn183, Asn179, and

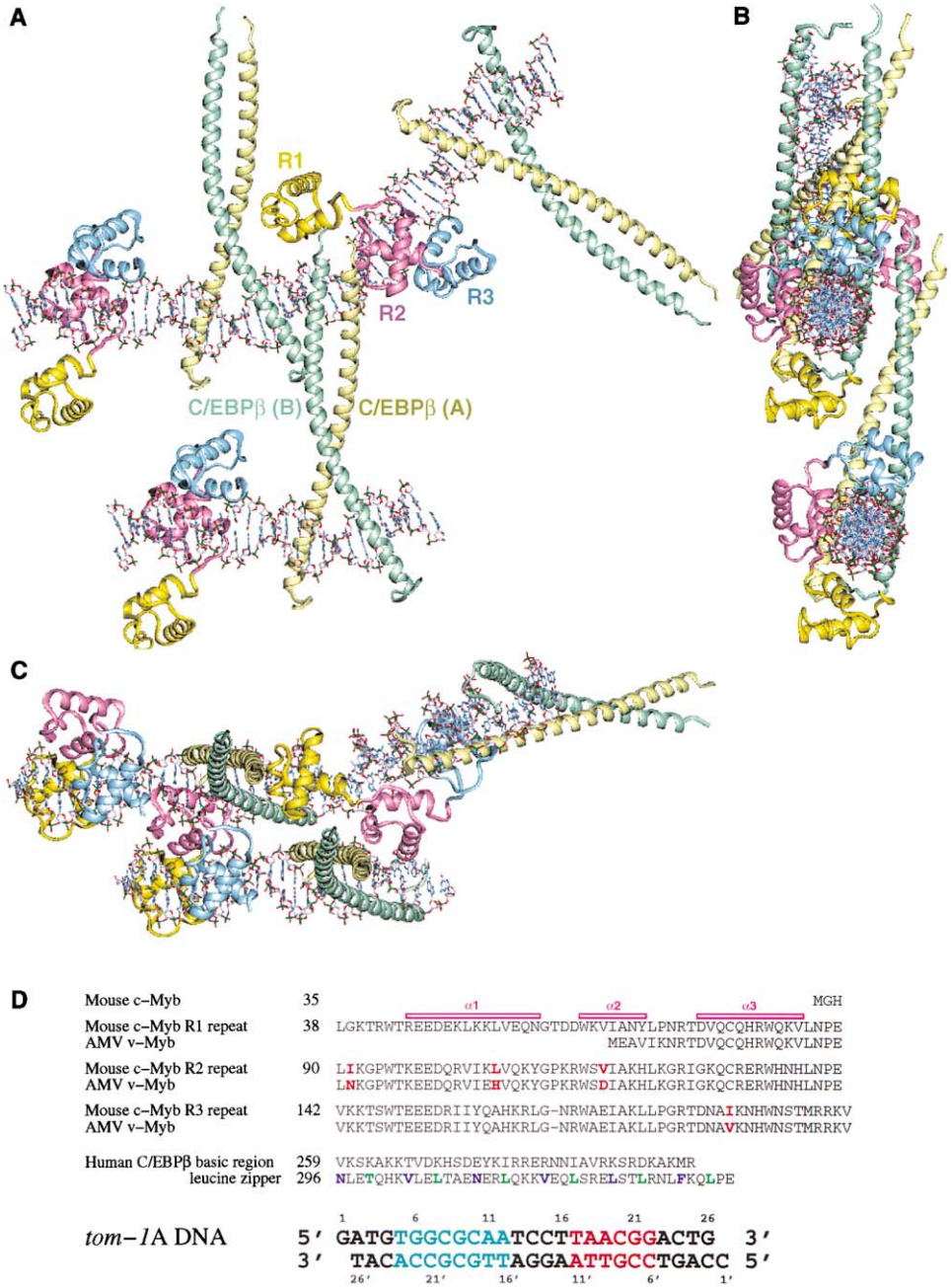

Figure 1. Overviews of Three Closely Packed c-Myb Complex I Molecules and Sequences of the Proteins and DNA Comprising the c-Myb and AMV v-Myb Complexes

(A–C) Closely packed c-Myb complex I molecules viewed from the front (A), from the side (B), and from the top (C). α helical regions within the proteins are shown as ribbons; the remaining parts are shown as tubes. c-Myb R1, R2, and R3 and C/EBPβ chains (A) and (B) are respectively colored dark yellow, pink, blue, yellow, and green. The DNA molecules are shown as a stick representation.

(D) Amino acid sequences of the c-Myb DBD, AMV v-Myb DBD, and C/EBPβ bZip region, and the nucleotide sequence of a 26 bp double-stranded DNA fragment used for crystallizations. The R1R2R3 domains of c-Myb and AMV v-Myb are aligned with the helical regions indicated on the top. The amino acid numbering for AMV v-Myb was adopted to correspond to that for c-Myb. The first and fourth positions of the heptad repeat in the C/EBPβ leucine zipper region are highlighted in cyan and green, respectively. In the DNA sequence, C/EBPβ and c-Myb binding sites are colored blue and red, respectively.

Lys182 of c-Myb R3 form bipartite hydrogen bonds with A18, A19, and G8′ bases, respectively, while Glu132 and Lys128 of c-Myb R2 form hydrogen bonds with C20 and G22 bases, respectively. The geometry of the recognition of C20 by the side chain of Glu132 is especially notable. While one oxygen from the Glu132 carboxyl group makes a hydrogen bond with the N4 nitrogen of C20, the other is packed against the C5 carbon of C20. Thus, consistent with the earlier study on the methylation-controlled promoter binding of Myb (Klempnauer,

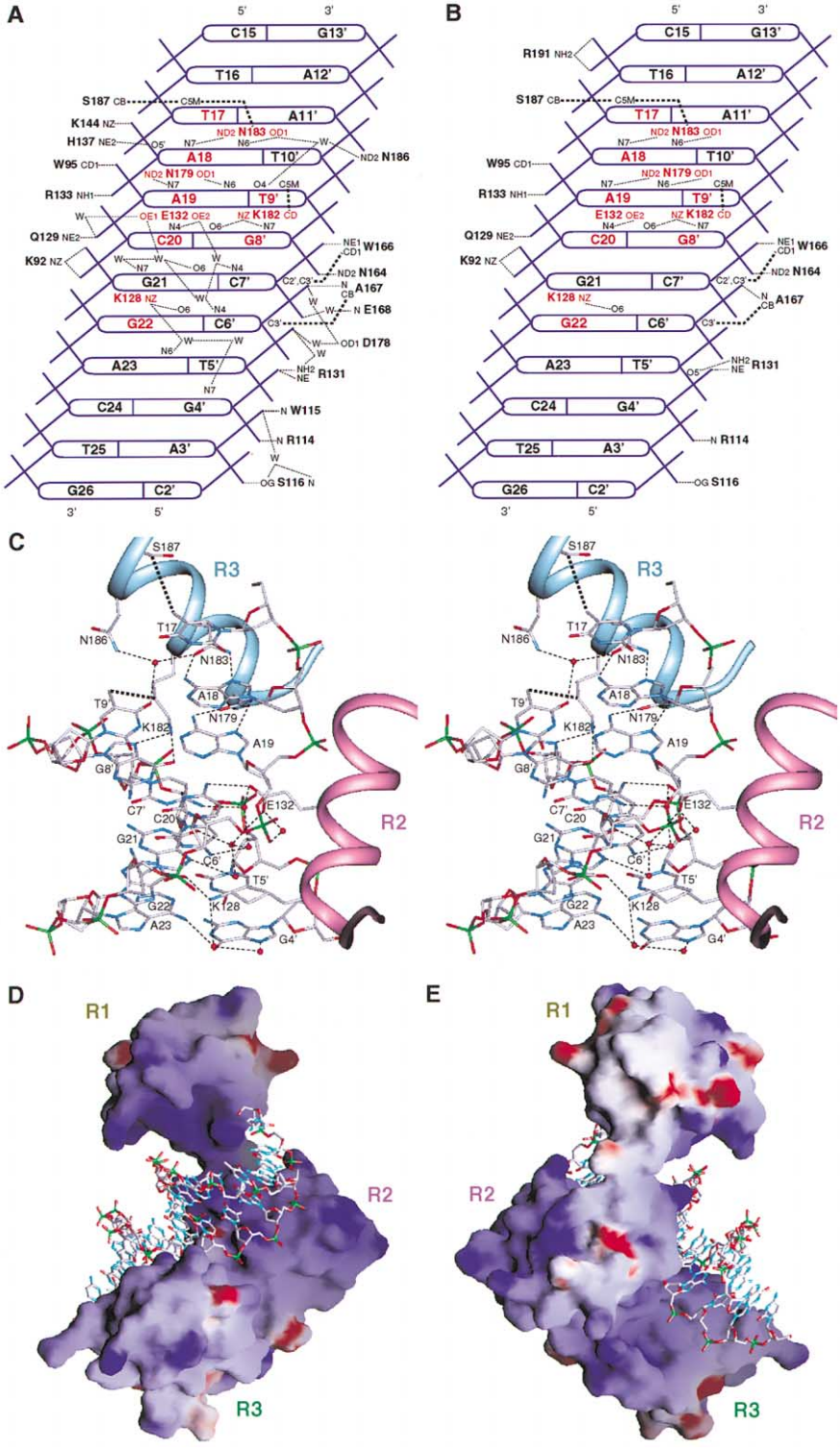

Figure 2. DNA Recognition by c-Myb and AMV v-Myb

(A and B) Schematic representations of DNA recognition by c-Myb (A) and AMV v-Myb (B). Dashed and solid lines depict intermolecular hydrogen bonds and van der Waals contacts, respectively. DNA bases labeled in red are involved in direct interactions with proteins.

(C) Stereo view of specific interactions between c-Myb and DNA bases. The peptide backbone of c-Myb is drawn as a pink or blue tube in the R2 and R3 regions, respectively. Thin and bold dotted lines depict intermolecular hydrogen bonds and van der Waals interactions, respectively. Water molecules are shown as red balls.

(D and E) Electrostatic surface potential of DNA-bound c-Myb R1R2R3 viewed from the front (D) and back (E); positively and negatively charged areas are colored blue and red, respectively.

1993; Tanikawa et al., 1993), methylation at the C5 carbon of the cytosine in the fourth position of the Myb consensus site would be expected to disrupt the interaction of the cytosine with Glu132 and weaken the binding affinity of c-Myb for DNA. In addition to the hydrogen bonding, van der Waals contacts between the methylene parts of the side chains of Asn183 and Ser187 and the methyl group of T17, and between the methylene part of the side chain of Lys182 and the methyl group of T9′ are observed. The first of these is thought to contribute to the pyrimidine preference in the first position of the Myb consensus sequence (Oda et al., 1997).

Water-mediated Myb–DNA interactions are also observed within the c-Myb complex (Figures 2A and 2C). A water molecule bridging the side chains of Asn183 and Asn186 is bound to the T9′ base, and the side chains of Glu132 and Lys128 also provide water-mediated interactions with DNA bases. Earlier studies by us showed that Myb binding is lost if a guanine is substituted at the C24 position (Figure 2A) (Tanikawa et al., 1993; Ogata et al., 1996). Given the structure of the c-Myb complex, the partial base limitation at this position may be explained by the water-mediated G4′ base recognition by the side chain of Lys128. Another study has shown that the sequence "YAACGN" can also serve as a Myb consensus sequence, as can "YAACNG" (Ording et al., 1996). In the case of the former, the side chain of Lys128 would be able to interact with the fifth position guanine with only a minor conformational change.

Contribution of c-Myb R1 to the c-Myb–DNA Interaction

Truncation of R1 reduces the binding affinity of c-Myb for DNA 5- to 6-fold (Tanikawa et al., 1993; Dini and Lipsick, 1993; Ording et al., 1994). Within the c-Myb complex, R1 covers the major groove and phosphate backbone of the DNA at a position adjacent to the R2 binding site, but makes no direct contacts with the DNA (Figures 1A–1C, 2D, and 2E), which is consistent with our previous studies (Tanikawa et al., 1993; Ogata et al., 1994, 1995). Calculation of the electrostatic surface potential of R1R2R3 revealed that the large positively charged surface of R1 is positioned facing the DNA major groove and the phosphate backbone (Figures 2D and 2E). The long-range electrostatic interaction between R1 and the DNA likely increases the stability of the c-Myb–DNA complex: the labile nature of the interaction between R1 and the DNA would allow R1 to continue to interact with a deformed DNA region, as in Figure 1A, where the DNA is bent as a consequence of c-Myb binding C/EBPβ (see below). This explanation is consistent with the finding of Ganter et al. (1999) that DNA binding activity and the *trans*-activation capacity of R1-truncated Myb is more easily affected by the local structure of DNA. These authors also suggested that DNA bending in the region interacting with R1 is important for efficient *trans*-activation by Myb proteins, which supports the functional relevance of c-Myb–C/EBPβ induced DNA bending observed in crystals.

Structural Changes in c-Myb R2 Induced by AMV-Type Mutations

Comparison of DNA-bound c-Myb R2R3 with AMV v-Myb R2R3 reveals significant structural differences in R2, but little difference in R3 (Figure 3A). The α2 helix of v-Myb R2 is shifted to the C-terminal side along the helical axis, as compared with that in c-Myb. This shift is caused by the I91N and/or L106H mutations. Leu106 in c-Myb is partially buried in the hydrophobic core of R2 and stabilizes the positions of Tyr110, Ile118, and His121, while His106 in AMV v-Myb inserts into a different part of the R2 hydrophobic core to relieve a steric hindrance involving Ile118, causing a conformational change in the side chain of Ile118 and a 2.5 Å shift in the position of the α2 helix in R2. The side chain of His106 in AMV v-Myb also makes a hydrogen bond with the Lys113 backbone, stabilizing a peptide bond linking Lys113 and Arg114, which fluctuates in the DNA free state of c-Myb (Ogata et al., 1995, 1996) and only becomes ordered upon DNA binding (Figure 3E and Ogata et al., 1994; Sasaki et al., 2000). Substitution of Ile91 in c-Myb with an Asn also contributes to the shift of the α2 helix in AMV v-Myb R2. Within the structure of c-Myb, the side chain of Ile91, which is located at the N terminus of R2, is packed toward the backbone oxygen of Lys123 at the C-terminal side of the α2 helix in R2, thereby supporting the position of the α2 helix. By contrast, Asn91 in AMV v-Myb hydrogen bonds to the backbone of Lys123, reducing the distance between the N terminus and the C-terminal side of the α2 helix in R2.

Unlike the I91N and L106H mutations, the V117D mutation also found in AMV v-Myb does not affect the disposition of the secondary structural elements in R2, but, through hydrogen bonds, stabilizes the side chain conformation of Arg114, the backbone of which is involved in DNA binding (Figure 3A).

Thus, these point mutations found in AMV v-Myb R2 change the packing mode of the residues in the hydrophobic core of R2 and make additional hydrogen bonds, which may affect the stability of this domain. We found the conformation-stabilizing effect of the mutations for the R2 domain by measuring the melting points of the wild-type and the AMV v-Myb R2 domains using the CD melting experiments: the obtained *T*m values were 39.7 ± 0.1°C (ΔH_v = 122 ± 1 kJ/mol) and 42.8 ± 0.1°C (ΔH_v = 160 ± 2 kJ/mol) for the wild-type R2 and the AMV v-Myb R2, respectively. This structural stabilization of R2 by AMV-type mutations may explain why AMV v-Myb is less sensitive to SH-specific modifications than c-Myb (Brendeford et al., 1997, 1998).

Effect of the AMV-Type Mutations on the c-Myb–DNA Interaction

We next examined the effects of AMV-type point mutations of c-Myb R2 on DNA binding activity. Comparison of the structures of the c-Myb and AMV v-Myb complexes shows their DNA recognition modes to be very similar (Figures 2A and 2B). There are, however, a few significant differences around the interaction site between the α1–α2 loop of Myb R2 and the phosphate backbone of the DNA, which, within the c-Myb complex, includes a protein backbone–DNA minor groove interaction. Within the AMV v-Myb complex, distances between the Arg114 and Trp115 backbone nitrogens and the G4′ phosphate oxygens are 3.4 Å and 4.4 Å, respectively, while the corresponding distances in the c-Myb complex are 2.7 Å and 3.2 Å (Figure 3B). These positional changes

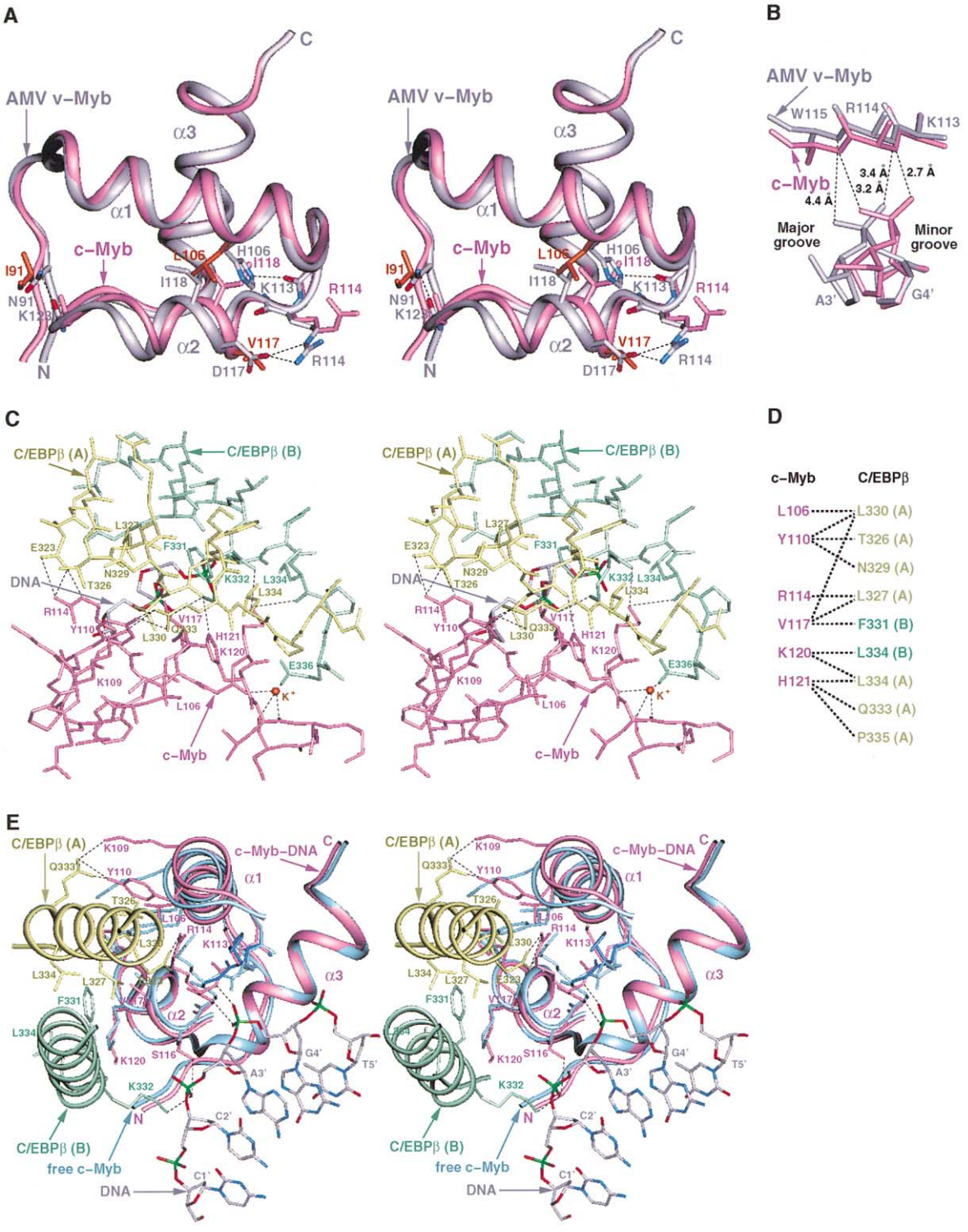

Figure 3. Structural Differences between c-Myb R2 and AMV v-Myb R2 and Close-Up Views of the Interactions among c-Myb, C/EBPβ, and DNA

(A) Stereo view of the superimposed R2 domains within c-Myb (pink) and AMV v-Myb (gray) complexes. The peptide backbones are drawn as tubes, and the side chains of residues that are mutated or exhibit different conformations in AMV v-Myb are drawn as sticks.

(B) A close-up view of the interactions between the Arg114 and Trp115 backbones and the DNA phosphate oxygens at G4′ within the c-Myb and AMV v-Myb complexes.

(C) Stereo view of the c-Myb–C/EBPβ interaction site. Intermolecular hydrogen bonds and K^+-mediated interactions are represented by dotted lines. Parts of c-Myb and C/EBPβ chains A and B are drawn as pink, yellow, and green sticks, respectively. The part of the DNA backbone interacting with the C/EBPβ leucine zipper region is also shown. The metal binding sites of R1, R2, and R3 were confirmed by their high-resolution crystal structures (T.T. et al., submitted).

Table 1. Kinetic and Dissociation Constants of c-Myb$_{38–193}$ or its Mutants Binding to DNA

c-Myb$_{38–193}$	DNA	K_D ($\times 10^{-8}$M)	k_a ($\times 10^6 M^{-1}s^{-1}$)	k_d ($\times 10^{-2}s^{-1}$)
Wild-Type	*tom-1A*[a]	3.53 ± 0.27	1.59 ± 0.22	5.61 ± 0.59
	mim-1[b]	0.164 ± 0.031	8.60 ± 0.80	1.40 ± 0.13
I91N	*tom-1A*	2.54 ± 0.12	3.18 ± 0.14	8.06 ± 0.04
	mim-1	0.170 ± 0.054	14.9 ± 3.8	2.43 ± 0.15
L106H	*tom-1A*	5.29 ± 0.01	2.56 ± 0.45	13.6 ± 2.5
	mim-1	0.388 ± 0.098	10.2 ± 1.0	3.89 ± 0.60
V117D	*tom-1A*	1.64 ± 0.13	4.44 ± 0.28	7.27 ± 1.05
	mim-1	0.125 ± 0.053	13.7 ± 3.7	1.62 ± 0.27
I91N/L106H	*tom-1A*	4.46 ± 0.06	2.85 ± 0.50	12.7 ± 2.4
	mim-1	0.382 ± 0.164	13.0 ± 3.6	4.66 ± 0.74
I91N/L106H/V117D	*tom-1A*	183 ± 60	0.0315 ± 0.0074	5.51 ± 0.55
	mim-1	2.26 ± 0.36	2.12 ± 0.59	4.68 ± 0.58

[a] 5′-CAATCCTTAACGGACTGAGG-3′.
[b] 5′-TACATTATAACGGTTTTTTA-3′.

in the Myb–DNA interface are correlated with the shift of the α2 helix of R2 described above, as well as with a conformational change in the bound DNA.

Previously, EMSA studies showed that AMV-v-Myb-type mutations in the Myb DBD destabilize the Myb–DNA complex (Brendeford et al., 1997), and that the DNA binding affinity of the AMV v-Myb DBD is more sensitive to the specific Myb consensus site flanking sequence, which affects the DNA conformation, than is c-Myb DBD (Ganter et al., 1999). The present structural data are well supported by these earlier findings. AMV-v-Myb-type mutations in the c-Myb DBD weaken the interaction between the backbone of the α1–α2 loop of R2 and the phosphate backbone of the DNA, which would be compensated for by DNA deformation.

To examine the effect of AMV-v-Myb-type mutations on the interaction between the Myb DBD and the DNA more precisely, we performed a series of surface plasmon resonance experiments. Five AMV-v-Myb-type point mutants of c-Myb$_{38-193}$ were prepared (I91N, L106H, V117D, I91N/L106H, and I91N/L106H/V117D), after which their binding affinities for the *mim-1* (Myb binding site A) and *tom-1A* promoter DNAs were measured (Table 1). While each of these mutations within R2 had some subtle effects on Myb–DNA binding, the three point mutations cooperatively reduced DNA binding activity, probably due to the positional changes around the α1–α2 loop–DNA minor groove interaction site described above. Remarkably, compared with the case of the *tom-1A* promoter, the impairment effect on the Myb-DNA interaction by the three point mutations seems to be partially compensated by the possible DNA deformation at the flanking T tract sequence of the Myb consensus site in the case of the *mim-1* promoter (Myb binding site A).

Interaction of C/EBPβ with DNA-Bound c-Myb

Figures 1A–1C, 3C, and 3D show the interaction between the c-Myb DBD in one c-Myb complex and the C-terminal region of C/EBPβ in another. Parts of the coiled-coil region of C/EBPβ chains A and B interact with the α1 and α2 helices of c-Myb R2 to form a motif resembling a four-helix bundle. The C/EBP family has a longer leucine zipper region than other basic leucine zipper proteins; the C-terminal region of the leucine zipper is extended by one heptad repeat. Within the c-Myb complex, this extended C-terminal leucine zipper region assumes a coiled-coil formation upon binding to c-Myb; within the v-Myb complex, by contrast, this region is partially unstructured and there is no interaction between C/EBPβ and v-Myb. The surface area buried between C/EBPβ and c-Myb–DNA is 1438 Å^2, which is within the range of values observed in other functional protein-protein interactions (Janin, 1997).

The C-terminal part of C/EBPβ chain A lies between the α1 and α2 helices of c-Myb R2 and forms a polar interaction network, while the C-terminal part of C/EBPβ chain B extends the interaction network by covering the remaining exposed area of the α2 helix and the c-Myb-bound DNA, proceeding to the groove between c-Myb R1, and R2. Arg114, Lys109, Tyr110, His121, K^+, Lys120, and c-Myb-bound DNA, in that order, make a circular polar interaction surface with C/EBPβ chains A and B, as follows: the side chain of Arg114 in the α1–α2 loop of c-Myb R2 makes bipartite salt bridges with the side chain of Glu323 in C/EBPβ chain A, stabilizing the conformation of the α1–α2 loop, which interacts with the DNA backbone. The side chains of Lys109 and Tyr110 in the α1 helix of c-Myb R2 make hydrogen bonds with the side chain of Gln333 in C/EBPβ chain A, and the side chain of His121 in the α2 helix of c-Myb R2 is hydrogen bonded to the backbone of Leu330 of C/EBPβ chain A. The K^+ mediates interactions between the backbone oxygens of Ala119, Leu122, and Arg125 in the α2 helix and α2α3 loop regions of c-Myb R2 and the side chain of Glu336 in C/EBPβ chain B. The side chain of Lys120 forms hydrogen bonds with the backbone atoms of Phe331 and Leu334 in C/EBPβ chain B. Around the c-Myb-bound DNA molecule, the side chain of Lys332 in C/EBPβ chain B makes a salt bridge with the

(D) Summary of the intermolecular van der Waals interactions between c-Myb and C/EBPβ.
(E) Stereo view of the c-Myb–C/EBPβ-DNA interaction site highlighting the interactions involved in stabilization of the α1–α2 loop of c-Myb R2. The peptide backbones of DNA-bound c-Myb (pink) and C/EBPβ chains A (yellow) and B (green) are drawn as tubes. Free c-Myb R2 (blue) is superimposed on the DNA-bound c-Myb R2. An alternative position for the disordered portion of the α1–α2 loop of the free c-Myb R2 is colored dark blue.

phosphate backbone of the DNA, while the side chain of Arg328 in the same chain interacts with the DNA phosphate via water molecules. The positions of Lys332 and Arg328 are conserved as basic residues among c-Myb-interacting C/EBP family members (C/EBPα, β, δ, and ϵ), and together these two residues provide a basic potential surface oriented toward the DNA.

Inside the polar interaction area, hydrophobic residues from c-Myb R2 and C/EBPβ chains A and B form van der Waals contacts. Interacting within this hydrophobic region are Leu106, Tyr110, the methylene part of Arg114, Val117, the methylene part of Lys120, and His121 from c-Myb R2; Thr326, Leu327, the methylene part of Asn329, Leu330, the methylene part of Glu333, Leu334, and Pro335 from C/EBPβ chain A; and Phe331 and Leu334 from C/EBPβ chain B. The site of interaction in c-Myb R2 includes two residues that are mutated in AMV v-Myb, and nearly corresponds to the hydrophobic patch that was previously predicted to be an interaction site for other Myb binding proteins (Ogata et al., 1995).

To confirm that the c-Myb–C/EBPβ interactions observed in the crystallized structure really exist in solution, we performed GST pull-down assays under DNA-free conditions using a GST-fused wild-type or mutated c-Myb DBD and the C/EBPβ C-terminal region containing the bZip region (Figure 4A). GST-c-Myb$_{1\text{-}193}$ and GST-c-Myb$_{38\text{-}193}$ efficiently bind to C/EBP$\beta_{259\text{-}345}$, and an R1-truncated c-Myb DBD (GST-c-Myb$_{90\text{-}193}$) exhibits only a slight reduction in affinity for C/EBPβ (Figure 4B). In contrast, AMV v-Myb DBD (GST-v-Myb$_{66\text{-}193}$), which contains the three point mutations in R2, fails to interact with C/EBPβ (Figure 4B). Like C/EBP$\beta_{259\text{-}345}$, C/EBP$\beta_{259\text{-}336}$, which was used for the present crystallographic analyses, also retains c-Myb binding affinity (Figure 4C). By contrast, truncation of seven residues from C/EBP$\beta_{259\text{-}336}$ to form C/EBP$\beta_{259\text{-}329}$ almost eliminates c-Myb binding activity under this condition, due to partial deletion of the c-Myb binding site. C/EBPβ-MUT$_{259\text{-}345}$, which contains four mutations (E323A/L330A/F331A/Q333A) of residues involved in c-Myb recognition within the crystal structure, also exhibits reduced c-Myb binding affinity. In these cases, all mutated C/EBPβ fragments used retain the capacity for homodimerization and binding to DNA (data not shown). Thus, consistent with the crystal structures, c-Myb interacts with the C-terminal region of leucine zipper of C/EBPβ in solution, whereas AMV v-Myb does not.

Structural Basis for Disruption of the Interaction of c-Myb and C/EBPβ by AMV-Type Mutations

c-Myb is known to physically interact with C/EBPϵ, the bZip region of which is highly homologous to that of C/EBPβ (Verbeek et al., 1999). Although AMV v-Myb was reported to interact with C/EBPβ (Mink et al., 1996), the v-Myb protein used in the study had the back mutations to the c-Myb-type DBD, indicating that R2 of the v-Myb protein they used contained no mutation. That the c-Myb DBD specifically interacts with C/EBPβ, while the AMV v-Myb DBD does not, suggests that the C/EBPβ binding affinity of AMV v-Myb is weaker than that of c-Myb, which can be attributed to the structural change in the C/EBPβ interaction surface of R2. To examine the effect of AMV-type mutations on C/EBPβ binding activity in solution, we performed GST pull-down assays using c-Myb mutants with various combinations of the AMV-type mutations. As shown in Figure 4D, the I91N and L106H mutations each drastically impair c-Myb–C/EBPβ binding. As C/EBPβ interacts with both the α1 and α2 helices of c-Myb R2, the positional shift of the α2 helix in R2 induced by the I91N or L106H mutations would be expected to alter the C/EBPβ binding surface, impairing the interaction between C/EBPβ and the mutated Myb.

As mentioned above, K^+ is involved in the interaction between Glu336 in C/EBPβ chain B and the peptide backbone extending from the α2 helix to the α2–α3 loop of c-Myb R2. In the AMV-v-Myb complex, the nearly regular triangle orientation formed by the backbone oxygens of Ala119, Leu122, and Arg125, which mediates K^+ binding, is significantly distorted by the shift of the α2 helix in R2, and the ion is absent. This may also contribute to the reduction in Myb–C/EBPβ binding affinity.

Val117 of c-Myb R2 makes a number of van der Waals contacts with C/EBPβ (Figures 3C and 3D). Unexpectedly, the V117D mutation found in AMV v-Myb does not impair C/EBPβ binding activity, but rather slightly enhances it. Based on a modeling study, it is predicted that loss of van der Waals contacts between Val117 and C/EBPβ would be energetically compensated for by formation of a salt bridge between the substituted Asp117 in Myb R2 and Arg328 in C/EBPβ chain B. In addition, Asp117 may interact with Phe331 in C/EBPβ chain B through π-orbitals in their side chain groups.

It is notable that these structural data, as well as the results of GST pull-down assays, correlate well with the phenotypes of cells infected by *v-myb* genes containing the various combinations of the mutations described (Introna et al., 1990).

Interaction between c-Myb and C/EBPβ Bound at a Distance from One Another on the *mim-1* Promoter

Within the c-Myb complex, the protein–protein interaction is not between c-Myb and C/EBPβ bound to the same DNA fragment, but between these molecules bound to different fragments. This raises the possibility that when bound to sites on the promoter that are well apart from one another, these two transcriptional regulatory factors are nonetheless able to directly interact by mediating DNA loop formation. To test whether such DNA loop formation actually occurs, we carried out a series of atomic force microscopy (AFM) experiments using c-Myb$_{38\text{-}193}$, C/EBP$\beta_{259\text{-}336}$, and a *mim-1* promoter DNA fragment. The *mim-1* promoter is one of the best characterized promoters of c-Myb target genes, and the *mim-1* gene is *trans*-activated by c-Myb but not by AMV v-Myb (Ness et al., 1989; Kowenz-Leutz et al., 1997). The promoter contains three c-Myb binding sites (A, B, and C at base positions -147, -186 and -208, respectively) (Ness et al., 1989), two C/EBPβ binding sites (at base positions -65 and -169) (Ness et al., 1993; Burk et al., 1993), and several putative Ets binding sites (Dudek et al., 1992). Among all of these, only c-Myb binding site A and the two C/EBPβ binding sites are reportedly important for *trans*-activation of the *mim-1* gene (Ness et al., 1993; Burk et al., 1993). In these experiments, we

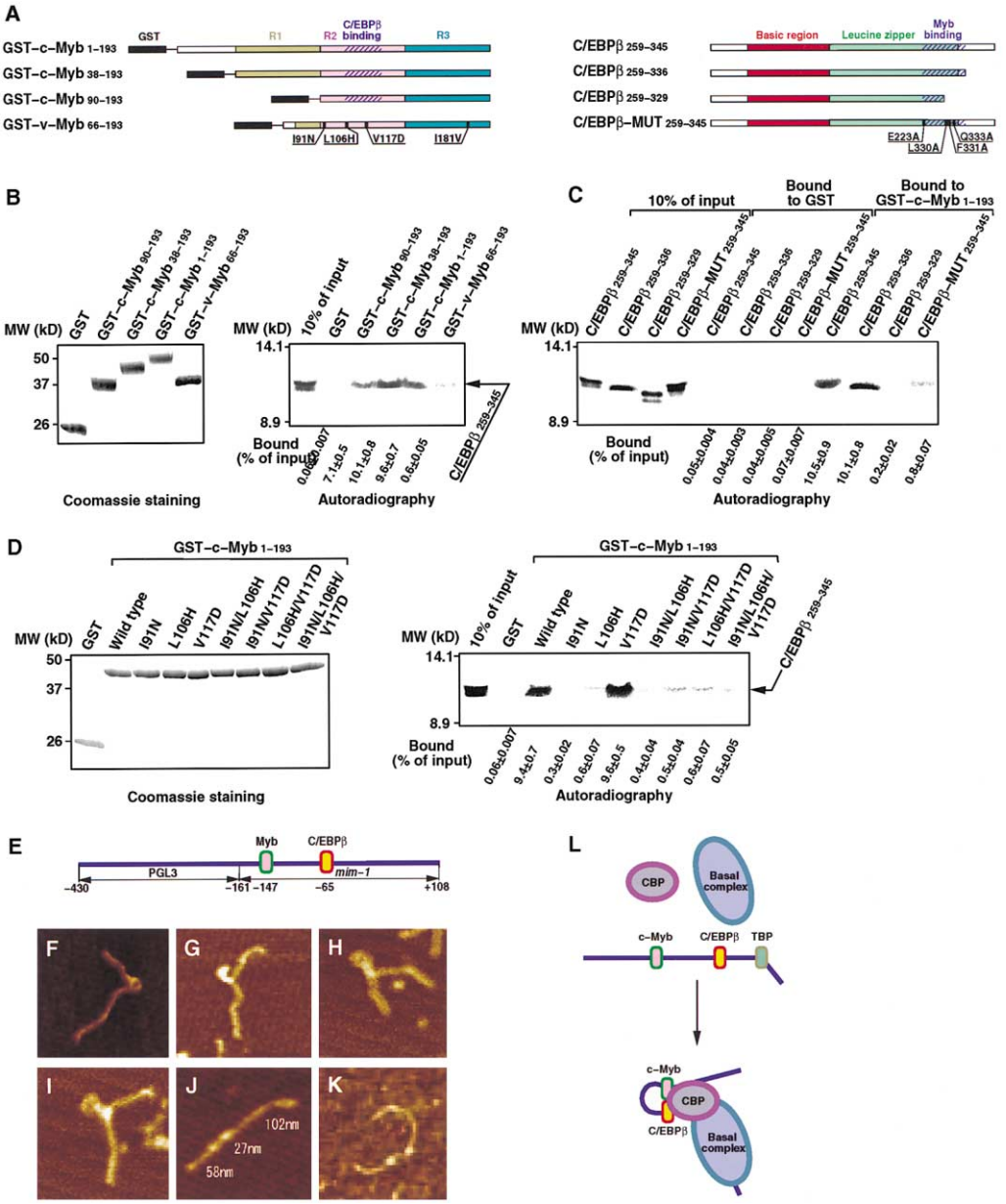

Figure 4. Examination of c-Myb-C/EBPβ Interaction and DNA Loop Formation Induced by c-Myb and C/EBPβ Interacting from Separated Sites on the *mim-1* Promoter

(A) Schematic diagram showing GST-fused c-Myb and C/EBPβ fragments and their mutants used in the GST pull-down assays.

(B) GST pull-down experiment examining the interactions between various GST-fused Myb protein fragments and C/EBP$\beta_{259\text{-}345}$. Left panel: GST-fused Myb proteins were analyzed by SDS-PAGE followed by Coomassie Blue staining. Right panel: binding of in vitro-translated ^{35}S methionine-labeled C/EBP$\beta_{259\text{-}345}$ to GST-fused Myb proteins was detected by autoradiography. The amounts of the bound C/EBP$\beta_{259\text{-}345}$ are shown under each line.

(C) GST pull-down experiment examining the interactions between GST-fused c-Myb$_{1\text{-}193}$ and various C/EBPβ protein fragments. Left four lanes: 10% input of in vitro-translated ^{35}S methionine-labeled C/EBPβ proteins. Center four lanes: binding of labeled C/EBPβ proteins to GST. Right four lanes: binding of labeled C/EBPβ proteins to GST-fused c-Myb$_{1\text{-}193}$. The amounts of the bound C/EBPβ mutants are shown under each line.

(D) GST pull-down experiment examining the interactions between various GST-fused c-Myb$_{1\text{-}193}$ mutants and C/EBP$\beta_{259\text{-}345}$. Left panel: GST-fused Myb proteins were analyzed by SDS-PAGE followed by Coomassie Blue staining. Right panel: binding of in vitro-translated ^{35}S methionine-labeled C/EBP$\beta_{259\text{-}345}$ to the GST-fused Myb proteins was detected by autoradiography. The amounts of bound C/EBP$\beta_{259\text{-}345}$ are shown under each line.

(E) Schematic diagram of the DNA fragment used for AFM experiments.

(F–I) Representative AFM images showing the c-Myb$_{38\text{-}193}$–C/EBP$\beta_{259\text{-}336}$–*mim-1* promoter DNA complex with loop formation.

(J) Representative AFM image of the v-Myb$_{66\text{-}193}$–C/EBP$\beta_{259\text{-}336}$–*mim-1* promoter DNA complex.

(K) Representative AFM image of the c-Myb$_{38\text{-}193}$–C/EBP$\beta_{259\text{-}329}$–*mim-1* promoter DNA complex.

(L) Schematic representation of proteins bound to a straight *mim-1* promoter and the stereospecific complex formed by the interaction of c-Myb and C/EBPβ.

used a *mim-1* promoter DNA fragment spanning a region from nucleotide position −161 to +108, which includes the C/EBPβ binding site at position −65 and Myb binding site A at position −147. For convenient observation of the DNA molecule, the promoter fragment was extended with DNA sequences from vector pGL3 having no binding sites for Myb or C/EBPβ (Figure 4E).

Figures 4F–4I show representative AFM photomicrographs of the c-Myb$_{38-193}$–C/EBPβ$_{259-336}$–*mim-1* promoter complex with loop formation. Out of 63 DNA fragments bound to both c-Myb$_{38-193}$ and C/EBPβ$_{259-336}$, 47 fragments (75% of total) exhibit loop formation. A more extensive AFM micrograph is presented as supplementary material (see Supplemental Figure S1, available online at http://www.cell.com/cgi/content/full/[108]/1/57/DC1). By contrast, when we used v-Myb$_{66-193}$ or C/EBPβ$_{259-329}$, in which the heterodimerization sites have been truncated (Figure 4A), the two proteins bind to DNA, but without a preference for DNA loop formation between the two protein binding sites (Figures 4J and 4K). For example, out of observed 25 v-Myb$_{66-193}$–C/EBPβ$_{259-336}$–*mim-1* promoter complexes, all DNA fragments had no loop, and out of 38 c-Myb$_{38-193}$–C/EBPβ$_{259-329}$–*mim-1* promoter complexes, only one DNA fragment exhibited a sharp bend. Thus, c-Myb could directly bind to C/EBPβ via the interaction observed in crystal, provided a loop is formed in the promoter DNA.

We then investigated the functional significance of the c-Myb-C/EBPβ interaction using a luciferase assay to assess the synergistic *trans*-activation of the *mim-1* gene (Figure 5). QT6 cells (a quail fibroblast cell line) were transfected with a luciferase reporter containing the 350-bp *mim-1* promoter region (nucleotides −242 to +108) (*mim-1*[242]luc), which contains the three Myb binding sites and two C/EBPβ binding sites, together with the Myb and/or C/EBPβ expression plasmids, and the resultant luciferase activity was measured (Figure 5B). In these assays, we used a truncated form of Myb in which both the C-terminal 183-amino acids and the N-terminal 37-amino acids were removed (Myb$_{38-453}$), because this C-terminal truncated form has a higher *trans*-activating capacity than full-length Myb. By themselves, wild-type C/EBPβ (C/EBPβ$_{1-345}$) or a C-terminal truncated C/EBPβ form lacking part of the Myb-interacting region (C/EBPβ$_{1-329}$) activated the *mim-1* promoter only about 4- to 5-fold; by itself, c-Myb had no effect. A combination of c-Myb and wild-type C/EBPβ (C/EBPβ$_{1-345}$) increased *mim-1* promoter activity about 14.5-fold, indicating that the two proteins act synergistically. When the C-truncated C/EBPβ (C/EBPβ$_{1-329}$) was used together with c-Myb, the degree of activation was reduced to 8-fold. Furthermore, when the Myb protein containing the three R2 point mutations (I91N/L106H/V117D) found in AMV v-Myb (v-Myb$_{38-453}$ or v-Myb$_{66-453}$) was used, the synergistic interaction with C/EBPβ was lost. This is despite the fact that AMV v-Myb and C/EBPβ were previously reported to synergistically activate the *mim-1* promoter (Mink et al., 1996); however, the v-Myb protein used in that study contained back mutations to c-Myb-type DBD, making the R2 region like that of c-Myb.

Because the *mim-1* promoter used in the above-described experiment contained three Myb binding sites and two C/EBPβ binding sites, the possibility remained that the observed synergistic action was the result of

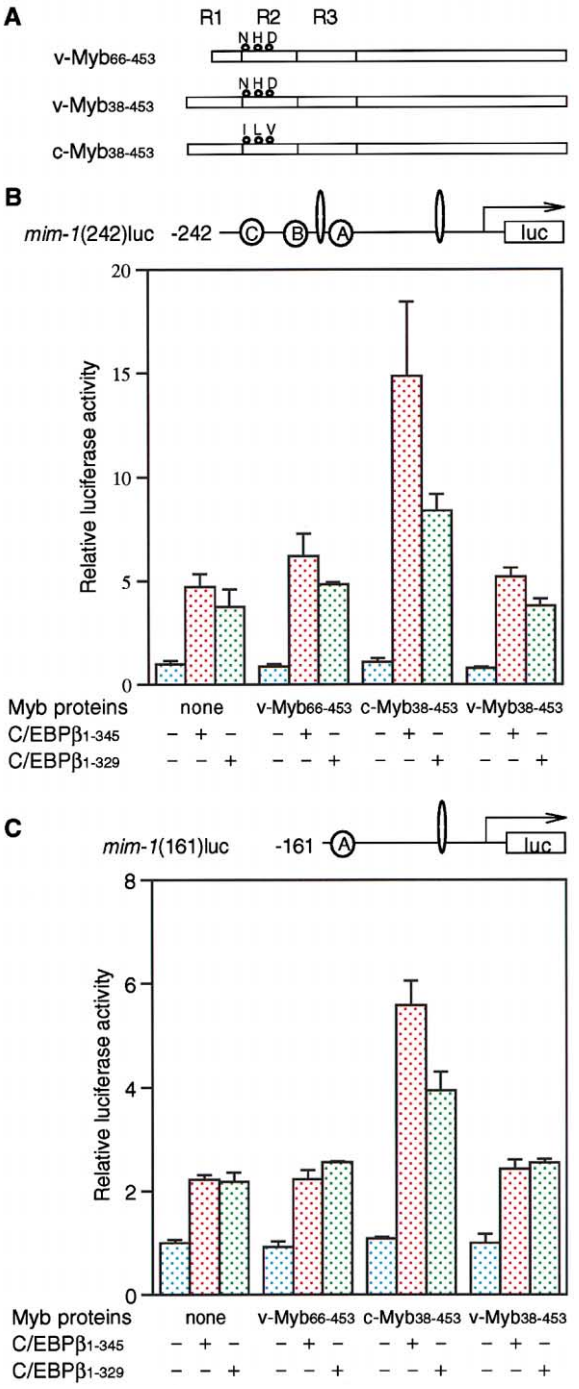

Figure 5. *trans*-Activation Experiments

(A) Definitions of the Myb proteins used for *trans*-activation experiments. Also see Experimental Procedures.

(B) Luciferase expression driven by the *mim-1*(242) reporter promoter. Locations of Myb (circle) and C/EBPβ (elongated ellipse) binding sites on the *mim-1*(242) promoter carried by the pGL3-mim242 reporter plasmid are also shown.

(C) Luciferase expression driven by the *mim-1*(161) reporter promoter. Locations of Myb (circle) and C/EBPβ (elongated ellipse) binding sites on the *mim-1*(161) promoter carried by the pGL3-mim161 reporter plasmid are also shown.

Table 2. Summary of X-Ray Experiments

Complex Type	v-Myb	c-Myb II	c-Mby I	c-Myb I-I1	c-Myb I-I2	c-Myb I-Br		
Crystal data								
a (Å)	109.9	62.7	41.7	41.5	41.6	41.5		
b (Å)	166.7	73.4	157.0	157.1	157.1	157.2		
c (Å)	39.6	161.7	55.9	55.6	55.5	55.2		
β (°)	90.0	90.0	100.2	100.3	100.3	100.1		
Space group	$P2_12_12$	$P2_12_12_1$	$P2_1$	$P2_1$	$P2_1$	$P2_1$		
Data collection								
Wavelength (Å)	1.0200	1.0400	0.97934	0.9195	0.97934	1.0200	0.9197	0.9191
Resolution (Å)	20–2.1	20–2.45	20–2.7	20–2.9	20–2.7	20–3	20–3	20–3
Observations	162864	205777	58631	38259	57964	41537	40671	38859
Unique reflections	42104	27451	18605	14141	18263	13279	13170	13051
Completeness (%)	97.3	99.0	96.0	93.4	96.8	97.5	96.7	96.0
R_{sym}	0.069	0.072	0.046	0.045	0.050	0.054	0.056	0.065
$I/\sigma(I)$	23.9	27.5	25.3	22.5	24.1	19.8	17.6	16.0
Phasing (3.2 Å resolution)				MIR		MAD		
R_{cullis}, isomorphous or dispersive/ anomalous				0.96	0.94	—/1.00	0.66/0.72	0.73/0.72
Phasing power, isomorphous or dispersive/anomalous				0.41	0.45	—/0.35	1.40/1.40	1.26/1.44
Figure of merit (each method)				0.19		0.42		
Figure of merit (combined)				0.45				
Refinement								
Resolution (Å)	20–2.23	20–2.45	20–2.8					
Reflections with $F > 0$	35692	27319	16664					
Atoms	3279	3266	3577					
R_{cryst}	0.245	0.229	0.222					
R_{free} (5% of reflections)	0.288	0.267	0.277					
Rms deviations								
bonds (Å)	0.005	0.005	0.006					
angles (°)	1.07	1.12	1.14					
Ramachandran plot (% of residues in regions)								
core	92.8	92.4	89.7					
additionally allowed	7.3	7.1	10.3					
generously allowed	0.0	0.4	0.0					

the interaction of c-Myb and C/EBPβ bound in close proximity to one another. To eliminate that possibility, we used another luciferase reporter containing the 269-bp *mim-1* promoter (nucleotides −161 to +108) (*mim-1*[161]luc), which has one Myb binding site at −147 and one C/EBPβ binding site at −65 (Figure 5C). Although the degree of activation was somewhat lower than that seen with *mim-1*(242)luc, the data are quite similar, indicating that the interaction of c-Myb and C/EBPβ bound to the promoter at a distance from one another plays a key role for the synergistic activation of transcription.

A Possible Mechanism for Protein Assembly from a Distance

We recently showed that conformational stabilization of a flexible "regulatory" loop, which interacts with the DNA minor groove, by a partner protein is a critical cooperative mechanism adopted by transcriptional regulatory proteins to increase their DNA binding affinity; the DNA complex containing AML1/Runx-1 and CBFβ is a good example (Tahirov et al., 2001a). Furthermore, structural comparisons of that complex with other multi-protein–DNA complexes suggest the proposed mechanism is a common element of protein assembly on promoter DNA. Consistent with that notion, a similar mechanism appears to be at work in the c-Myb–C/EBPβ–DNA complex described here. The regulatory α1–α2 loop of c-Myb R2 interacts with the DNA phosphate backbone from both the minor and major grooves via the backbone amide groups of Arg114 and Trp115 (Figures 3B and 3E). As we reported previously, the peptide bond linking Lys113 and Arg114 is flexible in the DNA-free state (Ogata et al., 1995, 1996; T.T. et al., submitted); however, when C/EBPβ binds to the c-Myb–DNA complex, major structural changes occur around the C terminus of α1 and the N terminus of α2 in R2, which ultimately affects the conformation of the α1–α2 loop, thereby stabilizing this part of c-Myb R2 (Figure 3E). In particular, the side chain of Arg114 in the α1–α2 loop, which interacts with the DNA minor groove, forms a salt bridge with the side chain of Glu323 in C/EBPβ chain A. AMV v-Myb–DNA binding escapes such regulation by C/EBPβ; instead, the substituted His106 and Asp117 residues, respectively, stabilize the conformations of the flexible peptide bond between Lys113 and Arg114 and the side chain of Arg114 (Figure 3A).

Implications of Synergistic Transcriptional Regulation

Most genes have promoter and enhancer regions that span hundreds of base pairs and contain multiple binding sites for a variety of transcriptional regulatory factors, often widely separated from one another. To create an appropriate surface for efficient interaction of transcriptional coactivators, however, a spatially close ar-

rangement of regulatory proteins bound to DNA seems to be required. In that regard, many Myb target genes also contain C/EBPβ binding sites, which are often widely separated from the Myb binding sites. The crystal structure of the c-Myb-C/EBPβ complex presented here, as well as the DNA loop created by the interaction of c-Myb and C/EBPβ and observed using AFM, support the notion that the direct interaction of c-Myb DBD with C/EBPβ bZip bound at a distance contributes to the generation of a molecular assembly suitable for synergistic activation of the target promoter. Both c-Myb and C/EBPβ bind to the coactivator CBP via their transcriptional activation domain (Dai et al., 1996; Oelgeschläger et al., 1996). Although the folding structures of their activation domains remain unknown, c-Myb-C/EBPβ complex formation may enhance binding of the CBP molecule (Figure 4L). Indeed, most likely, multiple enhancer binding proteins and coactivators interact via various domains to form a large protein complex, the so-called "enhanceosome," which synergistically stimulates transcription. Contributing to the formation of the enhanceosome is the capacity of transcription factors to interact despite being bound to widely separated sites.

In addition to the C/EBPβ binding site, some promoters of c-Myb target genes commonly contain the binding sites for Ets, AML1/Runx-1, or GATA-1 (Hernandez-Munain and Krangel, 1994; Bristos-Bray and Friedman, 1997; Zhang et al. 1997). It is therefore possible that, like C/EBPβ, these transcription factors also may interact with c-Myb via the DBD. Moreover, c-Myb DBD also reportedly interacts with several other factors, including p100, HSF3, and D-type cyclin (Ness, 1999; Kanei-Ishii et al., 1997; Ganter et al., 1998), suggesting that the c-Myb DBD may serve as a DNA/protein assembly module capable of mediating a wide array of interactions, probably in part via the C/EBPβ binding site in R2.

In conclusion, the present study provides important clues that increase our understanding of the regulation of *trans*-activation mediated by c-Myb and C/EBPβ and the dysregulation caused by oncogenic mutations. More broadly, it describes the structural basis of *trans*-activational synergy and the mechanism by which multiple transcriptional regulatory factors are assembled on promoter DNA for enhanceosome formation (Carey, 1998; Merika and Thanos, 2001).

Experimental Procedures

Structure Determinations

Polypeptide fragments of mouse c-Myb$_{38\text{-}193}$, AMV v-Myb$_{66\text{-}193}$, and human C/EBPβ$_{259\text{-}336}$ and C/EBPβ$_{273\text{-}336}$ were overexpressed in *Escherichia coli* BL21(DE3) using a T7 expression system and then purified. Sample preparation, crystallization, cryoprotection of native and heavy atom derivative crystals, and X-ray diffraction data collection made on a RIKEN beamline BL45XU at SPring-8 (Harima, Japan) have been described elsewhere (Tahirov et al., 2001b; Yamamoto et al., 1998). The compositions of the complexes were as follows. c-Myb complex I: c-Myb$_{38\text{-}193}$, C/EBPβ$_{259\text{-}336}$, and DNA; c-Myb complex I-I1: c-Myb$_{38\text{-}193}$, C/EBPβ$_{259\text{-}336}$, and DNA-I1; c-Myb complex I-I2: c-Myb$_{38\text{-}193}$, C/EBPβ$_{259\text{-}336}$, and DNA-I2; c-Myb complex I-Br: c-Myb$_{38\text{-}193}$, C/EBPβ$_{259\text{-}336}$, and DNA-Br; c-Myb complex II: c-Myb$_{38\text{-}193}$, C/EBPβ$_{273\text{-}336}$, and DNA; v-Myb complex: v-Myb$_{66\text{-}193}$, C/EBPβ$_{259\text{-}336}$, and DNA. The proteins used and the native DNA sequences are shown in Figure 1D, and the bromine (DNA-Br) and iodine (DNA-I1 and DNA-I2) derivatized DNA sequences are as described previously (Tahirov et al., 2001b).

The structure of c-Myb complex I was solved using a combination of the MIR and MAD methods. Two iodine positions were located initially for complex I-I2 by isomorphous difference Patterson search. SIR phases calculated with refined iodine positions of complex I-I2 were then used for isomorphous difference Fourier map calculation, enabling location of the iodine position in complex I-I1. MIR phases of iodine derivatives were used to locate the bromine positions in complex I-Br. The MAD and MIR phases calculated at 3.2 Å resolution were combined and used for density modification and phase extension from 4 Å to 2.8 Å with structural factors of the c-Myb complex I crystal. The resultant electron density map was slightly better than the modified MAD map, and enabled the protein backbones to be traced and all of the DNA bases and most of the DNA backbone to be fitted. All calculations were performed with CNS version 0.9a (Brünger et al., 1998). An initial model of c-Myb complex I was built using TURBO-FRODO software and then refined with CNS. The structures of c-Myb complex II and v-Myb complex were solved using the molecular replacement method with the refined structure of c-Myb complex I as a search model, and then refined with CNS. The structure of the entire c-Myb R1R2R3 domain was determined for c-Myb complex I. While in c-Myb complex II, the electron density map was interpretable starting from the third helix of R1, and no electron density was observed for the N-terminal 26 amino acids of v-Myb within the v-Myb complex. In addition, the N-terminal seven to nine amino acids of C/EBPβ were flexible within the structures of c-Myb complex I and v-Myb complex, making electron density uninterpretable. The data statistics used for the final refinement and for assessing the quality of the refined structures are summarized in Table 2. The figures containing the crystal structures were prepared using TURBO-FRODO, QUANTA, and GRASP (Nicholls et al., 1991) softwares.

CD Melting Experiments

Thermal denaturations of the wild-type R2 and the AMV v-Myb R2 domains were measured with CD while increasing the temperature at a rate of 0.75 K/min using a J-725 spectropolarimeter (Jasco, Japan). Samples were dissolved in 50 mM potassium phosphate buffer (pH 7.5) containing 50 mM KCl and 10 mM DTT. The concentration of each sample was 0.02 mM. Data were collected using cylindrical quartz cuvettes with a 1 mm path length, and the temperature was controlled with a thermoelectric (Peltier) temperature control system. Changes in ellipticity were monitored at 222 nm. The obtained experimental data of the thermal transition were curve fitted nonlinearly with the fixed ΔC_p value of 1.35 kJ K^{-1} mol^{-1} (Morii et al., 1999).

GST Pull-Down Assays

GST pull-down assays were performed using standard procedures. To express various GST-fused Myb proteins, plasmids were constructed using a PCR-based method with vector pGEX-4T-3 (Pharmacia). pSPUTK (STRATAGENE), a modified pSP65 vector, was used for the in vitro transcription/translation of C/EBPβ and its mutant proteins. The binding buffer used contained 20 mM HEPES (pH 7.5), 300 mM NaCl, 1 mM DTT, and 0.5% NP −40.

Surface Plasmon Resonance

Site-directed mutagenesis inducing point mutation of c-Myb$_{38\text{-}193}$ was carried out using a QuikChange Site-Directed Mutagenesis kit (STRATAGENE). The strategy for the expression and purification of the mutated Myb proteins was the same as that used with the wild-type c-Myb DBD. A BIAcore 2000 biosensor system (Pharmacia Biosensor, Uppsala) was used to measure the interaction between c-Myb$_{38\text{-}193}$ or its mutants and two double-stranded DNA fragments (5′-CAATCCTTAACGGACTGAGG-3′ and 5′-TACATTATAACGGTTTTTTA-3′) derived from the *tom-1A* and *mim-1* (Myb binding site A) promoters, respectively. The biotinated DNA was bound to the biosensor chip SA via streptavidin preimmobilized to dextran on the chip surface. The ligand was diluted to 0.2 μM in 100 mM potassium phosphate buffer (pH 7.4) containing 300 mM NaCl and 0.005% Tween 20, and applied to the sensor chip surface at a rate of 5 μl/min until 38 (for *tom-1A* DNA) and 25 (for *mim-1*DNA) resonance units were obtained. The running buffer was 100 mM potassium phosphate buffer (pH 7.4) containing 70 mM NaCl and 0.005%

Tween 20; as analytes, c-Myb$_{38-193}$ or its mutants were diluted to various concentrations in the same solution and then injected over the immobilized ligand at a rate of 100 μl/min until the injected volume reached 330 μl. Dissociation of the analytes was then measured by injecting the running buffer alone. All experiments were performed at 21°C. Data were analyzed with BIA evaluation version 3.0 using a nonlinear least squares method to obtain the association and dissociation rate constants (k_a and k_d, respectively). For this, the global fitting of the association and dissociation phases of the response curves using a 1:1 binding model was applied. The fittings were considered satisfactory if $\chi^2 \leq 3$. The equilibrium dissociation constants (K_D) were calculated from the equation $K_D = k_d/k_a$. The standard deviation was calculated from two experiments.

Plasmid Construction, Cell Culture, *trans*-Activation Assays and Western Blotting

Reporter gene constructs pGL3-mim242 and pGL3-mim161 were prepared by subcloning one of two chicken *mim-1* promoter fragments (nucleotide positions −242 to +108 or positions −161 to +108) upstream of the *Photinus pyralis* (firefly) luciferase gene in the pGL3-basic vector (Promega) via the KpnI-XhoI sites. As an internal control, the *Renilla reniformis* luciferase gene from vector pRL-TK (Promega) was subcloned downstream of the chicken cytoplasmic β-actin promoter in vector pact1 (Sakura et al., 1989) via the NheI-XbaI sites, yielding pact-RL. Expression vector pact-v-myb encoding v-Myb$_{66-453}$ has been described elsewhere (Sakura et al., 1989). Expression vector pact-ΔNCVR encoding c-Myb$_{38-453}$ was constructed by replacing the v-myb gene fragment encoding AMV v-Myb DBD in pact-v-myb with the c-myb gene fragment encoding c-Myb DBD via the NcoI-EcoRI sites. The expression vector encoding v-Myb$_{38-453}$ was constructed by mutagenesis of pact-ΔNCVR to express c-Myb$_{38-453}$ with three residue mutations—I91N, L106H, and V117D. The expression vectors for C/EBPβ$_{1-345}$ and C/EBPβ$_{1-329}$ were constructed by inserting a cDNA fragment encoding C/EBPβ$_{1-345}$ or C/EBPβ$_{1-329}$ into vector pact1 via the NcoI-XbaI sites. For these constructs, an NcoI restriction site within the cDNA encoding C/EBPβ was mutated beforehand without changing the amino acid sequence encoded.

QT6 cells (a quail fibroblast cell line) were cultured in Dulbecco's modified Eagle medium (DMEM) supplemented with 5% fetal calf serum, 2% chicken serum, and 2% triptose phosphate broth under a 5% CO_2 atmosphere at 37°C. DNA transfection of the cells was carried out using LIPOFECTAMINE2000 (GIBCO BRL) according to the manufacturer's instructions. Luciferase activities were measured using a Dual-Luciferase Reporter Assay System with a Turner Designs Luminometer (Model TD-20/20; Promega). The standard deviation was calculated from three experiments.

Samples of the cell lysate used for the luciferase assays were subjected to 10% SDS-PAGE and then electrophoretically transferred to Immobilon-P Transfer Membranes (MILLIPORE). The membranes were blocked for 1 hr in 5% skim milk (Difco) and then incubated for 2 hr with anti-C/EBP (Δ198, Santa Cruz) or anti-Myb (CT5; Sakura et al., 1989) polyclonal antibody. The blots were then washed three times with TBST buffer, incubated for 1 hr with anti-rabbit IgG (Santa Cruz), again washed three times with TBST buffer, and visualized using an ECL PLUS chemiluminescence system (Amersham Pharmacia, UK). All procedures were performed at room temperature; the transfer efficiency of the proteins was checked by staining the used membranes with amide black.

AFM Experiments

pGL3-mim161 was digested to obtain the BamHI-XhoI fragment, which was subjected to 2% agarose gel electrophoresis. A 531 bp DNA band was then cut and purified using a GFX PCR DNA Gel Band Purification Kit (Amersham Pharmacia, UK). The purified DNA sample was heated at 60°C for 5 min and then rapidly cooled on ice. Highly purified c-Myb$_{38-193}$ or v-Myb$_{66-193}$ plus C/EBPβ$_{259-336}$ or C/EBPβ$_{259-329}$ were mixed with the DNA in 10 mM Tris-HCl buffer (pH 7.2) for 5 min at room temperature and diluted 20 times to final concentrations of 2–3 nM DNA and 0.3–30 nM protein. Aliquots (10 μl) of the mixture were then dripped onto a mica substrate coated with spermine, rinsed with 1 ml of water, and blown with dry nitrogen gas. AFM analysis was carried out using a Nanoscope IIIa Multimode system (Digital Instruments Inc., Santa Barbara, CA) in the tapping mode at room temperature in air. Silicon cantilevers of 127 μm in length with a spring constant of 48N/m were purchased from Nanosensors (Wetzlar-Blankenfeld, Germany). Typical resonant frequencies of these tips were 340 kHz. The 512 × 512 pixel images were collected at a rate of two scan lines per second. The contour lengths of the protein-DNA complex were determined using Image Gauge (FUJIFILM, Japan).

Acknowledgments

We thank S. Akira for NF-IL6 cDNA, K. Takeyasu and A. Sarai for helpful comments, and M. Sato, N. Kamiya, T. Kato, I. Aoki, and M. Hosaka for generous support. AFM images were measured by T. Okada and R. Hirota of the Research Institute of Biomolecule Metrology, Tsukuba, Ibaraki, Japan. This research was in part supported by CREST (Core Research for Evolutional Science and Technology) of the Japan Science and Technology Corporation (JST) to K.O.

Received September 4, 2001; revised December 12, 2001.

References

Biedenkapp, H., Borgmeyer, U., Sippel, A.E., and Klempnauer, K.-H. (1988). Viral myb oncogene encodes a sequence-specific DNA-binding activity. Nature *335*, 835–837.

Brendeford, E.M., Myrset, A.H., Hegvold, A.B., Lundin, M., and Gabrielsen, O.S. (1997). Oncogenic point mutations induce altered conformation, redox sensitivity, and DNA binding in the minimal DNA binding domain of avian myeloblastosis virus v-Myb. J. Biol. Chem. *272*, 4436–4443.

Brendeford, E.M., Andersson, K.B., and Gabrielsen, O.S. (1998). Nitric oxide (NO) disrupts specific DNA binding of the transcription factor c-Myb in vitro. FEBS Lett. *425*, 52–56.

Bristos-Bray, M., and Friedman, A.D. (1997). Core binding factor cannot synergistically activate the myeloperoxidase proximal enhancer in immature myeloid cells without c-Myb. Mol. Cell. Biol. *17*, 5127–5135.

Brünger, A.T., Adams, P.D., Clore, G.M., DeLano, W.L., Gros, P., Grosse-Kunstleve, R.W., Jiang, J.-S., Kuszewski, J., Nigles, M., Panu, N.S., et al. (1998). Crystallography and NMR system: a new software suite for macromolecular structure determination. Acta Crystallogr. *D54*, 905–921.

Burk, O., Mink, S., Ringwald, M., and Klempnauer, K.-H. (1993). Synergistic activation of the chicken *mim-1* gene by *v-myb* and C/EBP transcription factors. EMBO J. *12*, 2027–2038.

Burk, O., Worpenberg, S., Haenig, B., and Klempnauer, K.-H. (1997). *tom-1*, a novel v-Myb target gene expressed in AMV- and E26-transformed myelomonocytic cells. EMBO J. *16*, 1371–1380.

Carey, M. (1998). The enhanceosome and transcriptional synergy. Cell *92*, 5–8.

Dai, P., Akimaru, H., Tanaka, Y., Hou, D.X., Yasukawa, T., Kanei-Ishii, C., Takahashi, T., and Ishii, S. (1996). CBP as a transcriptional coactivator of c-Myb. Genes Dev. *10*, 528–540.

Dini, P.W., and Lipsick, J.S. (1993). Oncogenic truncation of the first repeat of c-Myb decreases DNA binding in vitro and in vivo. Mol. Cell. Biol. *13*, 7334–7348.

Dudek, H., Tantravahi, R.V., Rao, V.N., Reddy, E.S.P., and Reddy, E.P. (1992). Myb and Ets proteins cooperate in transcriptional activation of the *mim-1* promoter. Proc. Natl. Acad. Sci. USA *89*, 1291–1295.

Fong, I.C., Zarrin, A.A., Wu, G.E., and Berinstein, N.L. (2000). Functional analysis of the human *RAG2* promoter. Mol. Immunol. *37*, 391–402.

Friedman, A.M., Fischmann, T.O., and Steiz, T.A. (1995). Crystal structure of *lac* repressor core tetramer and its implications for DNA looping. Science *268*, 1721–1727.

Ganter, B., Fu, S.l., and Lipsick, J.S. (1998). D-type cyclins repress transcriptional activation by the v-Myb but not the c-Myb DNA-binding domain. EMBO J. *17,* 255-268.

Ganter, B., Chao, S.T., and Lipsick, J. (1999). Transcriptional activation by the Myb proteins requires a specific local promoter structure. FEBS Lett. *460*, 401–410.

Hernandez-Munain, C., and Krangel, M.S. (1994). Regulation of the T-cell receptor δ enhancer by functional cooperation between c-Myb and core-binding factors. Mol. Cell. Biol. *14*, 473–483.

Howe, K.M., and Watson, R.J. (1991). Nucleotide preferences in sequence-specific recognition of DNA by c-myb protein. Nucleic Acids Res. *19*, 3913–3919.

Introna, M., Golay, J., Frampton, J., Nakano, T., Ness, S.A., and Graf, T. (1990). Mutations in *v-myb* alter the differentiation of myelomonocytic cells transformed by the oncogene. Cell *63*, 1287–1297.

Janin, J. (1997). Specific versus non-specific contacts in protein crystals. Nat. Struct. Biol. *4*, 973–974.

Kanei-Ishii, C., Sarai, A., Sawazaki, T., Nakagoshi, H., He, D.N., Ogata, K., Nishimura, Y., and Ishii, S. (1990). The tryptophan cluster: a hypothetical structure of the DNA-binding domain of the myb protooncogene product. J. Biol. Chem. *265*, 19990–19995.

Kanei-Ishii, C., Tanikawa, J., Nakai, A., Morimoto, R.I., and Ishii, S. (1997). Activation of heat shock transcription factor 3 by c-Myb in the absence of cellular stress. Science *277*, 246–248.

Klempnauer, K.-H. (1993). Methylation-sensitive DNA binding by v-myb and c-myb proteins. Oncogene *8*, 111–115.

Kowenz-Leutz, E., Herr, P., Niss, K., and Leutz, A. (1997). The homeobox gene *GBX2*, a target of the *myb* oncogene, mediates autocrine growth and monocyte differentiation. Cell *91*, 185–195.

Lipsick, J.S., and Wang, D.-M. (1999). Transformation by v-Myb. Oncogene *18*, 3047–3055.

Lutz, P.G., Houzel-Charavel, A., Moog-Lutz, C., and Cayre, Y.E. (2001). Myeloblastin is an Myb target gene: mechanisms of regulation in myeloid leukemia cells growth-arrested by retinoic acid. Blood *97*, 2449–2456.

Merika, M., and Thanos, D. (2001). Enhanceosomes. Curr. Opin. Genet. Dev. *11*, 205–208.

Mink, S., Kerber, U., and Klempnauer, K.-H. (1996). Interaction of C/EBPβ and v-Myb is required for synergistic activation of the *mim*-1 gene. Mol. Cell. Biol. *16*, 1316–1325.

Morii, H., Uedaira, H., Ogata, K., Ishii, S., and Sarai, A. (1999). Shape and energetics of a cavity in c-Myb probed by natural and non-natural amino acid mutations. J. Mol. Biol. *292*, 909–920.

Nakagoshi, H., Nagase, T., Kanei-Ishii, C., Ueno, Y., and Ishii, S. (1990). Binding of the c-Myb protooncogene product to the simian virus-40 enhancer stimulates transcription. J. Biol. Chem. *265*, 3479–3483.

Ness, S.A. (1999). Myb binding proteins: Regulators and cohorts in transformation. Oncogene *18*, 3039–3046.

Ness, S.A., Marknell, A., and Graf, T. (1989). The v-*myb* oncogene product binds to and activates the promyelocyte-specific *mim-1* gene. Cell *59*, 1115–1125.

Ness, S.A., Kowenz-Leutz, E., Casini, T., Graf, T., and Leutz, A. (1993). Myb and NF-M: combinatorial activators of myeloid genes in heterologous cell types. Genes Dev. *7*, 749–759.

Nicholls, A., Sharp, K.A., and Honig, B. (1991). Protein folding and association: insights from the interfacial and thermodynamic properties of hydrocarbons. Proteins *11*, 281–296.

Oda, M., Furukawa, K., Ogata, K., Sarai, A., Ishii, S., Nishimura, Y., and Nakamura, H. (1997). Identification of indispensable residues for specific DNA-binding in the imperfect tandem repeats of c-Myb R2R3. Protein Eng. *10*, 1407–1414.

Oelgeschläger, M., Janknecht, R., Krieg, J., Schreek, S., and Luscher, B. (1996). Interaction of the coactivator CBP with Myb proteins: effects on Myb-specific transactivation and on the cooperativity with NF-M. EMBO J. *15*, 2771–2780.

Ogata, K., Hojo, H., Aimoto, S., Nakai, T., Nakamura, H., Sarai, A., Ishii, S., and Nishimura, Y. (1992). Solution structure of a DNA-binding unit of Myb: A helix-turn-helix-related motif with conserved tryptophans forming a hydrophobic core. Proc. Natl. Acad. Sci. USA *89*, 6428–6432.

Ogata, K., Morikawa, S., Nakamura, H., Sekikawa, A., Inoue, T., Kanai, H., Sarai, A., Ishii, S., and Nishimura, Y. (1994). Solution structure of a specific DNA complex of the Myb DNA-binding domain with cooperative recognition of helices. Cell *79*, 639–648.

Ogata, K., Morikawa, S., Nakamura, H., Hojo, H., Yoshimura, S., Zhang, R., Aimoto, S., Ametani, Y., Hirata, Z., Sarai, A., et al. (1995). Comparison of the free and DNA-complexed forms of the DNA-binding domain from c-Myb. Nat. Struct. Biol. *2*, 309–320.

Ogata, K., Kanei-Ishii, C., Sasaki, M., Hatanaka, H., Nagadoi, A., Enari, M., Nakamura, H., Nishimura, Y., Ishii, S., and Sarai, A. (1996). The cavity in the hydrophobic core of Myb DNA-binding domain is reserved for DNA recognition and *trans*-activation. Nat. Struct. Biol. *3*, 178–187.

Ording, E., Kravik, W., Bostad, A., and Gabrielsen, O.S. (1994). Two functionally distinct half sites in the DNA-recognition sequence of the c-Myb oncoprotein. Eur. J. Biochem. *222*, 113–120.

Ording, E., Bergholtz, S., Brendeford, E.M., Jamin, N., and Gabrielsen, O.S. (1996). Flexibility in the second half-site sequence recognized by the c-Myb R2 domain – *in vitro* and *in vivo* analysis. Oncogene *13*, 1043–1051.

Sakura, H., Kanei-Ishii, C., Nagase, T., Nakagoshi, H., Gonda, T.J., and Ishii, S. (1989). Delineation of three functional domains of the transcriptional activator encoded by the c-*myb* proto-oncogene. Proc. Natl. Acad. Sci. USA *86*, 5758–5762.

Sasaki, M., Ogata, K., Hatanaka, H., and Nishimura, Y. (2000). Backbone dynamics of the c-Myb DNA-binding domain complexed with a specific DNA. J. Biochem. *127*, 945–953.

Schleif, R. (1992). DNA looping. Annu. Rev. Biochem. *61*, 199–223.

Tahirov, T.H., Inoue, T., Sasaki, M., Kimira, K., Morii, H., Fujikawa, A., Shiina, M., Sato, K., Kumasaka, T., Yamamoto, M., et al. (2001a). Structural analyses of DNA recognition by the AML1/Runx-1 Runt domain and its allosteric control by CBFβ. Cell *104*, 755–767.

Tahirov, T.H., Sasaki, M., Inoue, T., Fujikawa, A., Sato, K., Kumasaka, T., Yamamoto, M., and Ogata, K. (2001b). Crystals of ternary protein–DNA complexes composed of DNA binding domains of c-Myb or v-Myb, C/EBPα or C/EBPβ, and *tom-1*A promoter fragment. Acta Crystallogr. *D57*, 1655–1658.

Tanikawa, J., Yasukawa, T., Enari, M., Ogata, K., Nishimura, Y., Ishii, S., and Sarai, A. (1993). Recognition of specific DNA sequences by the c-*myb* proto-oncogene product-role of three repeat units in the DNA-binding domain. Proc. Natl. Acad. Sci. USA *90*, 9320–9324.

Tjian, R., and Maniatis, T. (1994). Transcriptional activation: a complex puzzle with few pieces. Cell *77*, 5–8.

Verbeek, W., Gombart, A.F., Chumakov, A.M., Muller, C., Friedman, A.D., and Koeffler, H.P. (1999). C/EBPε directly interacts with the DNA binding domain of c-myb and cooperatively activates transcription of myeloid promoters. Blood *93*, 3327–3337.

Weston, K. (1992). Extension of the DNA binding consensus of the chicken c-Myb and v-Myb proteins. Nucleic Acids Res. *20*, 3043–3049.

Weston, K., and Bishop, J.M. (1989). Transcriptional activation by the v-*myb* oncogene and its cellular progenitor, c-*myb*. Cell *58*, 85–93.

Wolberger, C. (1998). Combinatorial transcription factors. Curr. Opin. Genet. Dev. *8*, 552–559.

Yamamoto, M., Kumasaka, T., Fujisawa, T., and Ueki, T. (1998). Trichromatic Concept at SPring-8 RIKEN Beamline I. J. Synchrotron Rad. *5*, 222–225.

Zhang, X., Xing, G., Fraizer, G.C., and Saunders, G.F. (1997). Transactivation of an intronic hematopoietic-specific enhancer of the human Wilms' tumor 1 gene by GATA-1 and c-Myb. J. Biol. Chem. *272*, 29272–29280.

Accession Numbers

The atomic coordinates of c-Myb complexes I and II and v-Myb complex have been deposited in the Protein Data Bank with the ID codes 1h88, 1h89, and 1h8a, respectively.